Fire Technology, 59, 1115–1135, 2023

https://doi.org/10.1007/s10694-022-01251-0

Preheating Performance by Heating Film for the Safe Application of Cylindrical Lithium-ion Battery at Low Temperature

Wen Yang and Fei Zhou, State Key Laboratory of Mechanics and Control of Mechanical Structures, Nanjing University of Aeronautics and Astronautics, Nanjing 210016, China and National Key Laboratory of Science and Technology On Helicopter Transmission, Nanjing University of Aeronautics and Astronautics, Nanjing 210016, China*

Yuchen Liu and Xing Chen, National Key Laboratory of Science and Technology On Helicopter Transmission, Nanjing University of Aeronautics and Astronautics, Nanjing 210016, China

Received: 29 October 2021/**Accepted:** 6 April 2022/**Published online:** 23 April 2022

Abstract. The conductivity of the electrolyte and the kinetics of Li^+ inside lithium-ion batteries (LIBs) will decrease at low temperatures, which may promote the formation of lithium dendrite. The growing of lithium dendrites will penetrate the separator, and cause the internal short circuits and thermal runaway of cells. Thus, battery preheating is essential to improve the safety of LIBs. To investigate the temperature changes of battery during discharging and preheating at low temperatures, the electro-thermal model and the preheating model of LIBs at low temperature are established and verified based on the second-order equivalent circuit model. The internal resistance of battery decreases with the increase of temperature. Moreover, a battery module with polyimide flexible heating film is proposed, and the heating films are arranged on both sides of the battery symmetrically. When the power of heating films is 1 W, 3 W, and 5 W, it takes 395 s, 190 s and 126 s to preheat the battery temperature from − 10°C to 25°C, respectively. Additionally, different heating powers can be arranged in the heating process to reduce the heating time and temperature difference of battery. The research in this study contributes to the preheating of LIBs in cold regions, and has certain reference value.

Keywords: Lithium-ion battery, Preheating, Low temperature, Polyimide flexible film

1. Introduction

Lithium-ion batteries (LIBs) have been the main power supplies for electric vehicles (EV) with the advantages of high energy density, high working voltage and long service life [1, 2]. However, LIBs fire cause at least 124 EV accidents in 2020 according to the document of Analysis of Electric Vehicle Fire Accidents in 2020

*Correspondence should be addressed to: Fei Zhou, E-mail: fzhou@nuaa.edu.cn

provided by TELD, which is the largest charge service operator in China. Commercialized LIBs are generally consists of graphite anodes, lithium metal oxide cathodes and carbonate electrolytes. The charging and discharging of LIBs are the reversible transfer of Li^+ ion between the anode and cathode of the cell. The anodes and cathodes are separated by insulating separator to prevent short circuit of the cell [3]. Occasionally, the mechanical deformation and over-charge/over-discharge of the LIBs may cause the damage of the separator, resulting in the short circuit and temperature increase of the cell [4].The increasing of battery temperature accelerates the chemical reactions inside the cell, which leads to the rapid self-heating or thermal runaway (TR). In addition to the heat released by chemical reactions, the ejected battery material may be ignited in the air and cause deflagration [5, 6]. Moreover, the performances of LIBs are very sensitive to temperature, and the most suitable working temperature of LIBs is 20 °C and 40 °C [7, 8]. The performance and life of LIBs will be deteriorated significantly at low temperatures (below 0 °C) because the conductivity of electrolyte and the diffusion rate of Li^+ ions decreases, and the charge-transfer resistance at the electrolyte–electrode interface increases [9]. The risk of thermal runaway caused by continuous exothermic reaction in low temperature may be low [10]. However, when the LIBs charge and discharge in low temperature environment for long time, the kinetics of Li^+ ions is reduced and the Li^+ ions may be deposited on the surface of the electrode in the form of metal [11]. The deposition shape of lithium metal is dendritic, which is called lithium dendrite [12]. Then, the growing lithium dendrites may penetrate the separator, which may cause the internal short circuits. When the battery is short-circuited, it will generate huge heat in a short time, and the temperature of the battery will rise sharply and even results in the fires of LIBs. Therefore, to improve the fire safety and reduce the TR risk of LIBs, battery preheating is important for EVs operation in low temperature environment.

The methods of preheating battery at low temperature can be divided into internal preheating and external preheating. Internal preheating usually uses high battery impedance at low temperatures to generate a large amount of electrochemical heat inside the battery when battery charge and discharge. Internal preheating includes DC internal resistance preheating, AC internal resistance preheating, and mutual pulse preheating. The internal resistance of the battery at low temperature is several times higher than that at room temperature, and the heat generated by the internal resistance is increased [13]. Li et al. [14] combined the thermal model and the electrochemical impedance model to propose a low-temperature thermo-electric coupling model for lithium-ion batteries. The results showed that the optimal frequency range was distributed in the high-frequency area. The optimized heating strategy could achieve a temperature rise from − 20 °C to 0 °C in 520 s. Zhang et al. [15] embedded a thin nickel foil with certain resistance into the square battery as the internal heating element at low temperatures. The battery was heated from − 20 °C to above 0 °C in 12.5 s, which increased the temperature difference between the inside and the surface of the battery. However, the high-rate charging and discharging of the battery will aggravate the aging in the long run [16].

External heating usually uses a heat source outside the battery to generate heat, which can be divided into convection preheating and conduction preheating according to the heat transfer method. Convective heating typically uses hot air or liquid to heat battery from outside. Wang et al. [17] investigated the potential economic benefits of preheating the battery pack through the air heating strategy in the power system. As compared with the case without preheating process, the preheating strategy could limit the operating cost to 22.3% over 40 driving cycles at the ambient temperature of − 20°C. Zhu et al. [18] added three heaters in the pipeline-based liquid cooling system, which were powered by the charging pile. The results showed that the battery pack was heated from − 10°C to 2°C within 1157 s, and the temperature between batteries was 3.1 °C. Although the air heating has simple structure and good temperature uniformity, the heating rate is low and cannot meet the requirements of rapid preheating in low temperature environments [19]. Then, the liquid heating has high thermal conductivity and good heating rate, but the cost and leakage risk is high. Conduction preheating means that the heating installations are attached directly to the surface of the battery and exchange heat with the battery. Zhang et al. [20] compared the heating effect of the heating film placed on the side and bottom of the square battery pack. Under the same energy consumption, the side heating method made the battery system have higher temperature rise and better temperature uniformity. Lei [21] placed two wide-wire metal films in the middle of the battery module composed of three square 35Ah $LiMn_2O_4$ batteries. When the battery was preheated with 90 W heating film at − 40 °C for 15 min, the discharge capacity was restored to the room temperature level, and the charging capacity was restored to half of the room temperature level. Zhang et al. [22] proposed a battery preheating method combining phase change materials and heating films, and the heating films were attached on the two larger side surfaces of the battery. When the heating power was fixed at 20 W, it took about 613 s to heat up the battery from − 20°C to 10°C, while the temperature difference of battery was less than 5°C. The heating film shows high efficiency and strong adaptability to the battery structure in battery preheating. However, the battery is assumed not to discharge during preheating, and there is no heat generation inside the battery [22]. Actually, the heating film is usually provided energy by the battery, and the self-heating of battery during discharging should be considered. Moreover, the temperature of the battery rises during preheating, which will decrease the internal resistance and self-heating of battery. The electro-thermal model of LIBs at low temperature should be established.

The polyimide flexible (PI) heating film has advantages of high electro-thermal conversion efficiency, small size, simple structure, and convenient customization. Meanwhile, the burning point of polyimide is higher than 400°C, and the PI heating film can be directly pasted on the cylindrical battery for preheating. Thus, a battery module with PI heating film is proposed in this study. When the battery provides power to the PI film, the heat generated by the PI film and battery discharge is considered. The electro-thermal model and the preheating model of 18650 lithium-ion battery at low temperature are established based on the second-order equivalent circuit model (ECM), and the parameters of ECM are measured using the experiment of Hybrid Pulse Power Characterization. Then, the thermal

performance of battery that simulated by the MSMD module of FLUENT software is verified by experiment. Moreover, the effects of arrangement, heat power, and heat process of heating film on preheating performance are discussed.

2. Battery Electro-Thermal Model

2.1. Equivalent Circuit Model of Battery

The 18650 cylinder Li-ion battery with $LiNi_{0.8}Co_{0.1}Mn_{0.1}O_2$ as the cathode material is selected in this study. As compared with the single-stage Resistor-Capacitance (RC) circuit, the multi-stage RC circuit can reflect more voltage characteristics of battery. Complex electrochemical reactions are occurred in battery during the charging and discharging, and the second-order equivalent circuit model is selected to construct the electro-thermal model of battery as show in Fig. 1, which can improve the accuracy of simulation. Assuming that the discharge current is positive, the dynamic voltage (U_{cell}), current (I) and state of charge (SOC) can be expressed as [23, 24]:

$$U_{cell} = U_{ocv} - IR_0 - U_1 - U_2 \tag{1}$$

$$I = \frac{U_1}{R_1} + C_1\frac{dU_1}{dt} = \frac{U_2}{R_2} + C_2\frac{dU_2}{dt} \tag{2}$$

$$SOC = SOC_0 - \frac{\eta}{Q_t}\int_0^t I(t) \tag{3}$$

where U_{ocv} is the open circuit voltage, V; R_0 is the ohmic resistance, Ω; U_1 is the voltage of first parallel RC circuit, V, which represents the polarization voltage; U_2 is the voltage of second parallel RC circuit, V, which represents the concentration difference voltage; SOC_0 is SOC at the initial stage; η is the Coulomb efficiency coefficient, and Q_t is the battery capacity, Ah.

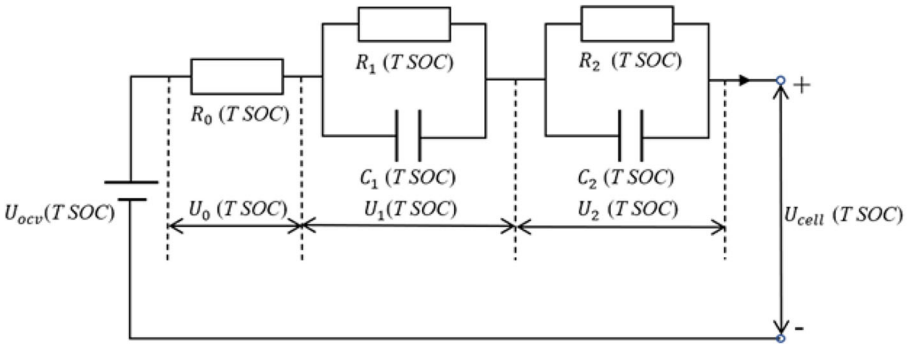

Figure 1. Second-order equivalent circuit model.

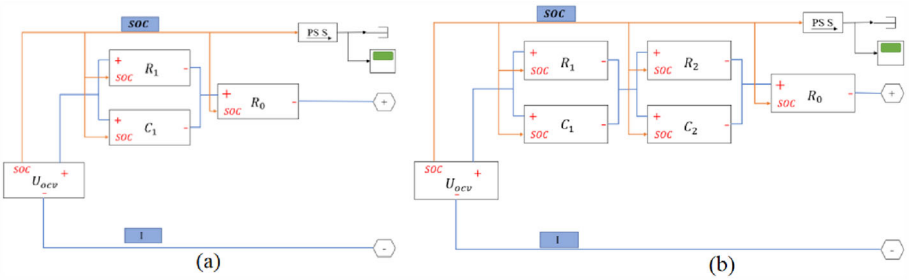

Figure 2. First-order (a) and second-order (b) RC ECM in Simulink.

The offline parameter identification is selected to calculate the parameters of second-order ECM. Offline parameter identification is the process that the polynomial fitting is used to identify the parameters based on the obtained experimental data, and its identification results are usually the fixed values, mappings, or functional relationships. In this study, the experiments of Hybrid Pulse Power Characterization (HPPC) are carried out at different temperatures to obtain experimental data [25]. However, it is difficult to directly identify the parameters of the second-order ECM using the offline parameter identification. The identification of the two RC circuit parameters may fail in the process of mutual coupling. Thus, the first-order ECM of battery is established firstly in Simulink as shown in Fig. 2a, which is used to identify the ohmic resistance R_0, polarization resistance R_1 and polarization capacitance C_1 of the battery. Then, a second-order ECM is established in Simulink, as shown in Fig. 2b, and the identified parameters of first-order RC equivalent circuit are set as its initial value. The diffusion resistance R_2 and diffusion capacitance C_2 are identified, and the parameters of R_0, R_1 and C_1 are slightly adjusted.

2.2. Governing Equations of the BTMS

The energy equation of heat transferring along cells is expressed as [26]:

$$\rho_b c_{p.b} \frac{\partial T_b}{\partial t} = \nabla \cdot (k_b \nabla T_b) + G(t) \tag{4}$$

where ρ is the density, kg m^{-3}, c_p is the specific heat capacity, J kg^{-1} $°C^{-1}$; k is the thermal conductivity coefficient, W m^{-1} °C $^{-1}$; T_b is the temperature of battery, °C; $G(t)$ is the thermal source term including battery and heating film, W m^{-3}.

During the discharging process of battery, the heat generated rate of battery is expressed as [27]:

$$q_{gen} = \frac{I}{Vol}\left[U_{OCV} - (\varphi_+ - \varphi_-) - T_b \frac{dU_{OCV}}{dT_b}\right] + \sigma_+ \nabla^2 \varphi_+ + \sigma_- \nabla^2 \varphi_- \tag{5}$$

where the q_{gen} is heat generated rate of battery,W m^{-3}; the $\sigma +$ is the effective electric conductivity of positive electrode, Ω^{-1}; $\sigma -$ is the effective electric conductivity of negative electrode, Ω^{-1}; φ_+ is the phase potentials of the positive electrode, V; $\varphi -$ is the phase potentials of the negative electrode, V; Vol is the volume of battery, m^3; T_b is the temperature of battery, °C; and $\frac{dU_{OCV}}{dT_b}$ is the entropy coefficient of battery, V $°C^{-1}$.

2.3. Polyimide Film and Power Calculation

PI heating film is made of polyimide film as the outer insulator and metal foil as the inner conductive heating element, which is pressed at high temperature and high pressure. The thickness of PI heating film is 0.5 mm, and the thickness of metal foil is only 0.05 mm. Thus, the physical properties of polyimide are selected as those of the heating film in this study. The structural and physical parameters of PI heating film are listed in Table 1. In order to reduce costs and simplify the model, the rectangular heating film was selected according to the preheating requirements of batteries at low temperatures as shown in Fig. 3. The length, width, and thickness of heating film are 50 mm, 25 mm, and 0.5 mm, respectively. The contact area between the heating films and the battery is 12.5 cm^2. When the battery is applied at high temperature, the battery needs heat dissipation. The exposure of some surfaces of the battery is conducive to the contact of cold air or radiator with the battery for heat exchange because of the low thermal conductivity of PI heating film. Then, two heating films are attached symmetrically on both sides of the battery, which can evenly heat the battery while leaving more exposed surfaces on the battery for heat dissipation. The preheating experiment diagram is shown in Fig. 4. The power of the heating film can be adjusted by using a PWM controller, which can control the working voltage loaded on both ends of the heating film. The T-type thermocouple sensor (measurement range: − 50 to 200 °C, measurement accuracy: ± 0.1 °C) is mounted on the surface of the battery symmetrically, and the temperature data are recorded by the paperless recorder.

Table 1
Basic Parameters of PI Heating Film

Parameters	Values
Thickness (mm)	0.5
Nominal power (W)	7
Nominal voltage (V)	12
Density (kg m^{-3})	1400
Specific heat capacity (J kg^{-1} $°C^{-1}$)	1090
Thermal conductivity coefficient (W m^{-1} $°C^{-1}$)	0.15
Working temperature (°C)	−50–200

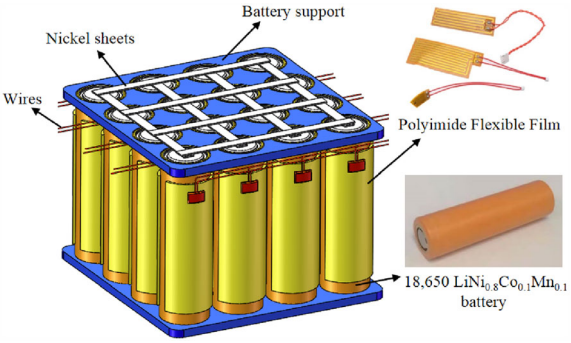

Figure 3. Battery model and PI heating film.

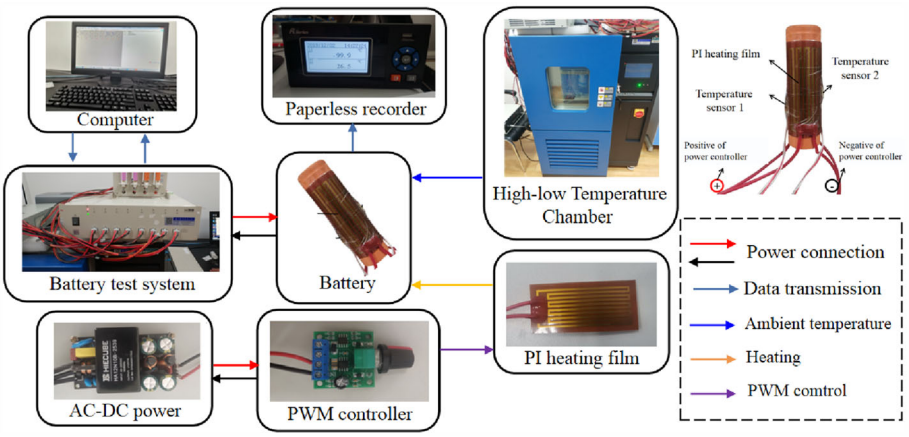

Figure 4. Experiment diagram of preheating.

According to the rated voltage and rated power, the working voltage, current and heat generated rate of heating film can be calculated by the following equations.

$$U = \sqrt{P \cdot R} = \sqrt{P \cdot \frac{12^2}{7}} = 4.54\sqrt{P} \tag{6}$$

$$I = \sqrt{\frac{P}{R}} = \sqrt{P \cdot \frac{7}{12^2}} = 0.22\sqrt{P} \tag{7}$$

$$q_{film} = P/V_{film} \tag{8}$$

where P is the rated power of heating film, W; R is the internal resistance of heating film, Ω; U is the voltage of heating film, V; I is the current of heating film, A;

q_{film} is the heat generated rate of heating film, W m^{-3}; and V_{film} is the volume of heating film, m^3.

The rated power of the heating film here is 7 W and the rated voltage is 12 V. When the heating powers are 1 W, 3 W and 5 W, the output voltage of PWM controller are 4.53 V, 7.85 V and 10.14 V, respectively. Meanwhile, the currents of heating film are 0.44 A, 0.768 A and 0.986 A, respectively. Then, the discharge currents of cell are 0.88A, 1.54 A, and 1.97 A in the process of battery preheating.

3. Parameter Identification of ECM

The experiments of Hybrid Pulse Power Characterization (HPPC) were carried out at different temperatures. The experiments are conducted in the thermal chambers (GP/T-50, GUANGPIN TEST EQUIPMENT Co., Ltd.) using battery test system (XINWEI, CT-4008, 5V12A, accuracy: 0.05%). The specific steps of HPPC were shown as:

(1) The battery was first charged at a constant current of 1C before the cell voltage reached 4.2 V and then charged at the constant voltage of 4.2 V until the current was lower than 0.09 A. Then, the battery was placed under 25 °C ambient temperature for 1 h.
(2) The battery was discharged at 1C constant current for 10 s, and rested for 40 s. Subsequently, it was charged at 1C constant current for 10 s, and rested for 40 s.
(3) After the battery was discharged at 1 C constant current for 6 min, which caused the SOC of the battery reduced by 10%, the battery was rested in the test temperature for 1 h again.
(4) The above discharge steps were repeated until the SOC of the battery was 0.

The offline parameter identification was carried out at different temperatures to identify the characteristic data (R_0, R_1, C_1, R_2, and C_2) according to the results of HPPC. The specific steps of identification in MATLAB/Simulink based on ECM were shown as:

(1) The current and voltage data were extracted in HPPC working conditions at different temperatures, and then these data were uploaded to the workspace in the MATLAB software.
(2) The first-order equivalent circuit model was established in MATLAB/Simulink, and the current and voltage data from the previous step was input into this model.
(3) The range of the restricted identification parameter was set to be greater than 0, and the parameters of R_0, R_1 and C_1 were identified using the parameter identification function of Parameter Estimation. In the process of parameter identification, Sum Square Errors (SSE) was used as the error convergence function by default.
(4) The first-order model is expanded into second-order model in MATLAB/Simulink, and the parameters identified in the first-order model are input into

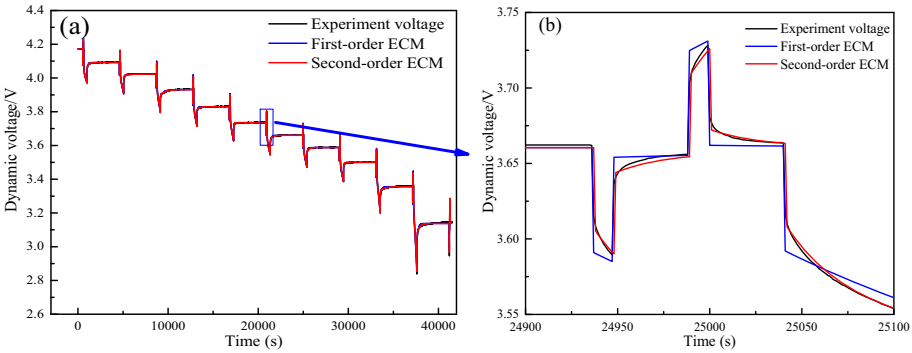

Figure 5. Identification voltage of the first-order and second-order ECM in 25 °C.

the second-order model as initial values. Then, the identification process is repeated to obtain the values of R_0, R_1, R_2, C_1, and C_2.

(5) The above identification steps are repeated at different temperatures to obtain the ECM parameters at different temperatures and SOC states.

Figure 5 is the identification voltage of HPPC working condition at ambient temperature of 25 °C. Figure 5b is the partial enlarged view of the dynamic voltage of Fig. 5a when the SOC of battery is 0.5. As compared with the first-order ECM, the second-order ECM can better describe the details of voltage changes.

After parameter identification, the equivalent resistance parameters at different temperatures are shown in Fig. 6a, 6b and 6c. It can be seen that the values of R_0, R_1 and R_2 increase with the decrease of temperature. When the ambient temperature reduces from 25 °C to 0 °C, the ohmic resistance R_0 increases from 0.02 Ω to 0.06 Ω at 0.5 SOC. However, the value of R_0 rises by 0.07 Ω while the ambient temperature reduces from 0 °C to -15 °C. The lower the ambient temperature, the greater the increase rate of battery resistance. The reason is that the conductivity of the battery electrolyte and solid electrolyte interface is reduced with the decrease of temperature. It proves that the offline parameter identification based on temperature changes conforms to the laws of physics. At the start and end of the discharge, the SOC change will have a significant impact on the values of R_0, R_1 and R_2. The identification accuracy is evaluated with error sum of squares (SSE) in Fig. 6d, and the maximum SSE is less than 0.18. Therefore, the identification accuracy is satisfied for the study requirements. The obtained parameters are used to calculate the heat generated rate of battery through the interpolation fitting. The fitted polynomials of ECM parameters at different temperatures are summarized in Appendix A.

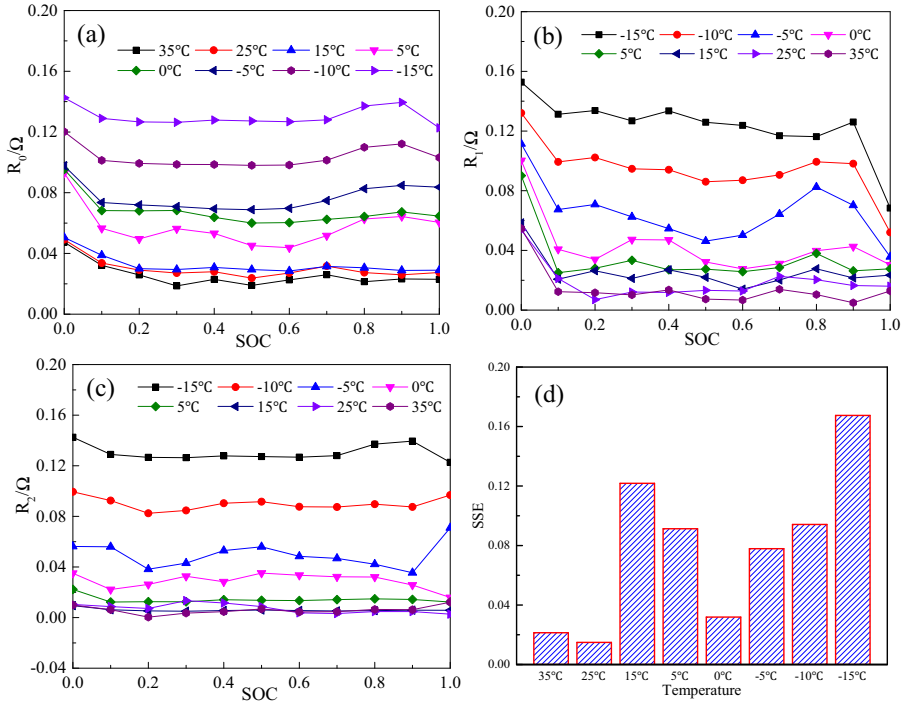

Figure 6. Identification parameters and SSE of ECM at different temperatures.

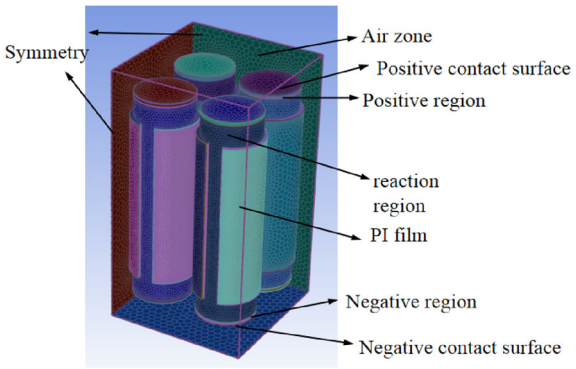

Figure 7. Simulation model of battery module.

4. Numerical Simulation and Verification

4.1. Heat Generation of Battery

According to the symmetrical structure of the battery module, the battery simulation model in the MSMD model of Fluent is established as shown in Fig. 7. The

Table 2
Properties of the Parts of the Battery [28, 29]

Properties	Reaction region	Positive region	Negative region
Diameter (mm)	18	18	18
Height (mm)	63	1	1
Density (kg/m^3)	2575.5	8030	8979
Thermal conductivity coefficient (W m^{-1} °C $^{-1}$)	5	387.6	300
Specific heat capacity (J kg^{-1} °C $^{-1}$)	1157.8	502.48	381
Conductivity ($\times$ 10^5 S/m)	354	833	580

properties of the 18,650 cylinder LIB with $LiNi_{0.8}Co_{0.1}Mn_{0.1}O_2$ are listed in Table 2. The positive current collector, negative current collector, and reaction material of battery correspond to the positive region, negative region, and reaction region in simulation model, respectively. The positive contact surface and negative contact surface are applied to set the series–parallel connection between multiple batteries. The contact surfaces between the reaction region and the positive/negative region are set as interior interface. The outer surface of the air zone is set as symmetry. It is assumed that the battery module is insulated from the outside environment. In this study, the average temperature of the battery module is used to verify the grid independence. The SIMPLE method is selected for numerical simulation, and the residual convergence of the energy equation and UDS diffusivity are set to 1.0×10^{-10} and 1.0×10^{-8}, respectively. The solution time step is set to 1 s, and the number of calculation steps is set to 200. The analysis model is divided into three grid numbers, which are 106537, 211478 and 460545. The relative deviations of the average battery temperature are 0.16% when the grid number changes from 211478 to 460545. Thus, the grid number of 211,478 is used in the following models.

At different ambient temperatures (− 10°C, − 5°C and 0°C), the surface temperature and voltage changes of the battery at different discharge rates (1C, 1.5C and 2C) in the test and simulation are compared in Fig. 8. According to the ambient temperature (− 10°C, − 5°C and 0°C), the discharge currents of 1C are set as 1.71 A, 1.82 A and 2.02 A, respectively. The terminal voltage of the battery decreases gradually with the discharge of battery, while the surface temperature of the battery increases. Then, with the increase of discharge rate, the discharge time is reduced and the maximum temperature of battery is raised. Especially, in the early discharge stage of 2 C-rate, the terminal voltage first decreases rapidly at ambient temperature of − 10°C, then gradually rises, and finally continues to decline. In this process, the surface temperature of battery increases by 15°C. In low temperature environment, the resistance of the battery change sharply with temperature. As the temperature of the battery increases, the resistance of the battery decreases, and the terminal voltage increases.

In the comparison of test and simulation at different ambient temperatures and discharge rates, the changes of terminal voltage and temperature changes are very similar. It can be seen from Table 3 that the maximum relative errors of terminal

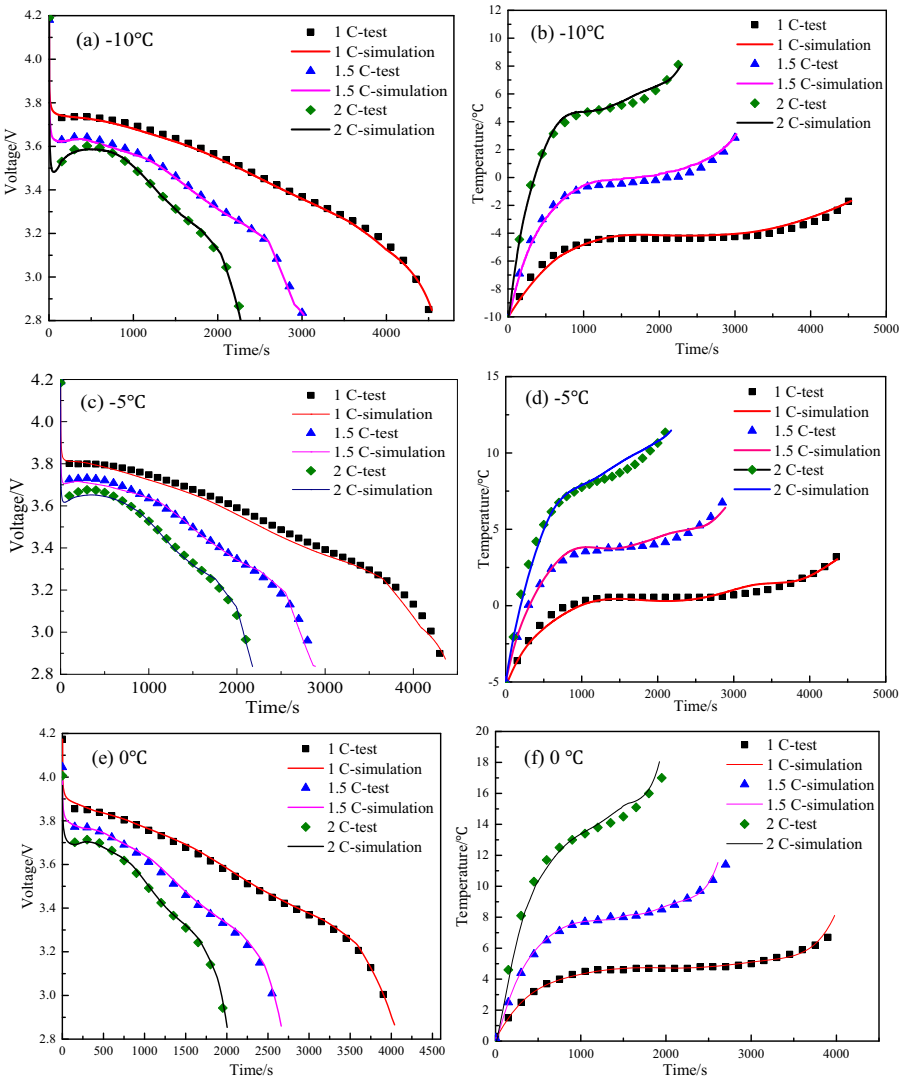

Figure 8. Comparison of test and simulation at different ambient temperatures and discharge rate.

voltage and surface temperature are 0.023 V and 0.5 °C, respectively. It indicates that the ECM of battery can adjust the internal parameters according to the SOC and temperature of battery, and the terminal voltage and surface temperature simulated by the model this study have high accuracy at low temperature.

Table 3
Maximum Relative Error of Terminal Voltage (V) and Surface Temperature (°C) at Different Temperatures and Discharge Rate

		Ambient temperature			
Parameter	Discharge rate	−10°C	−5°C	0°C	25°C
Terminal voltage (V)	1C	0.015	0.023	0.013	0.022
	1.5C	0.011	0.017	0.017	0.019
	2C	0.011	0.015	0.014	0.022
Surface temperature (°C)	1C	0. 3	0.3	0.3	0.2
	1.5C	0.4	0.2	0.3	0.3
	2C	0.3	0.5	0.3	0.3

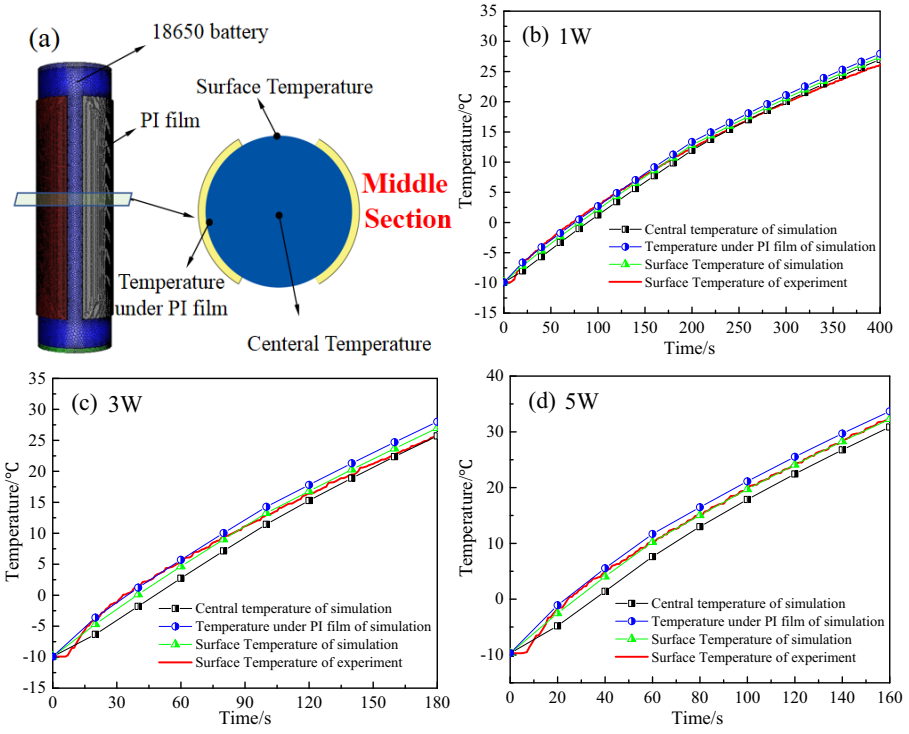

Figure 9. Simulation preheating model (a) and temperature change under 1 W (b), 3 W (c), and 3 W (d).

4.2. Preheating of PI Film

Two PI films were attached to the surface of the battery for preheating symmetrically, and simulation model of battery is shown in Fig. 9a. When the PI films preheat the battery at -10 °C with power of 1 W, 3 W and 5 W respectively, the

changes of the battery temperature are shown in Fig. 9 b-d. With the increase of heating power, the rise rate of the battery temperature increases gradually. In the middle section of the battery, the temperature under the PI film is the highest, and the minimum temperature is located at the center of the battery. The heat provided by PI films radiates from the films to the surrounding and the center of the battery, which cause the temperature rise of the battery. Meanwhile, the surface temperature of the battery is higher than the central temperature because the self-generated heat of the battery is very lower than that of PI film. The surface temperature of simulation was compared with the experimental data. The errors between test data and simulation data are less than 5%, which proves the rationality of the simulation model.

5. Effect of Preheating Strategy

5.1. *Effect of the Arrangement of Heating Film*

In order to explore the influence of the arrangement of heating film on the heating performance of the battery, the two kinds of arrangement cases are compared as shown in Fig. 10. In the symmetrical case, two PI films are pasted symmetrically on both sides. The sum of the contact area S_{sym} is 25 cm^2 calculated as in Eq. 9. In the spiral case, a PI heating film is attached spirally to the battery surface. The number of spiral turns is 3, and the height of the spiral line and the width of heating film is 14.6 mm and 14.3 mm, respectively. The contact area S_{spi} is around 25 cm^2 calculated as in Eq. 10. The heating power of the spiral arrangement PI film is 6 W, and the heating power of the two symmetrical arrangement heating films is 3 W respectively.

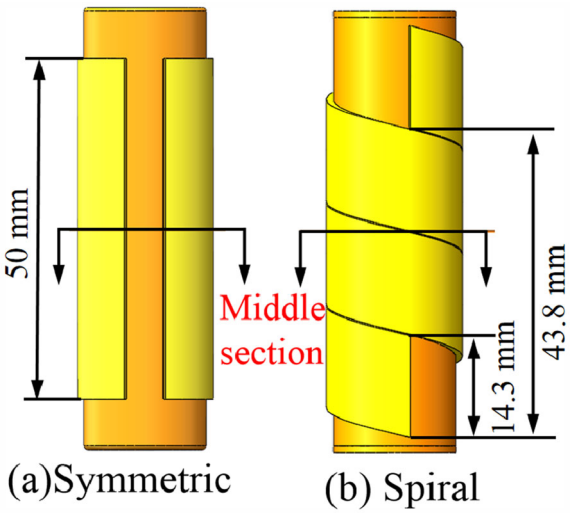

Figure 10. Different arrangement of heating film.

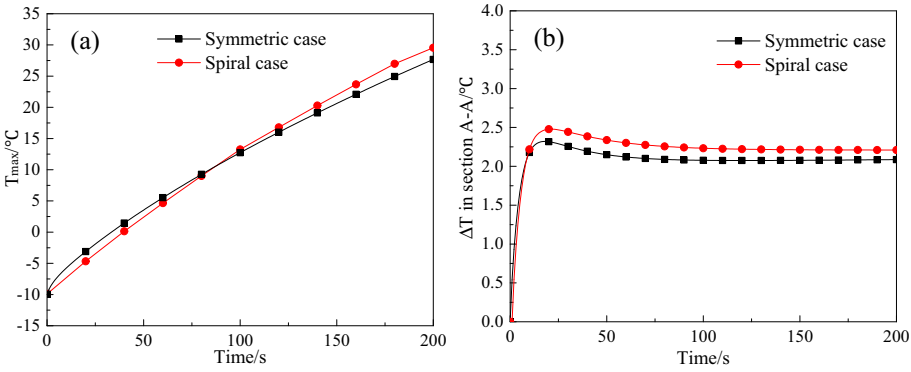

Figure 11. Maximum temperature and temperature difference in middle section.

$$S_{sym} = 2 \times l \times d = 2 \times 50mm \times 25mm = 2500mm^2 \tag{9}$$

$$S_{spi} = 3 \times \sqrt{(\pi \times D)^2 + s^2} \times 14.3 = 3 \times \sqrt{(\pi \times 18mm)^2 + 14.6mm^2} \times 14.3mm \approx 2500\ \text{mm}^2 \tag{10}$$

The temperature changes of battery on middle section are shown in Fig. 11. The maximum temperature (T_{max}) of battery on middle section increases with preheating time, and the values of T_{max} in symmetric case and spiral case are 27.7 °C and 29.2 °C, respectively. The temperature difference (ΔT) of the battery on middle section increases rapidly and then decreases slightly. After discharge for 200 s, the ΔT values for symmetric case and spiral case are 2.1 °C and 2.2 °C, respectively. The temperature contours of battery in two cases are shown in Fig. 12 at ambient temperature of -10 °C after preheating the battery for 200 s. The temperature at both ends of the battery is significantly lower than that in the middle, while the temperature on the surface of the battery is higher than that in the center. The uniformity of temperature distribution of symmetric case is better than spiral case.

5.2. Effect of the Power of Heating Film

Preheating time, temperature difference and power consumption of battery are important evaluation values of the preheating performance. In this section, the effect of preheating power (1 W, 3 W and 5 W) of heating film on the preheating performance is studied at ambient temperature of -10 °C as shown in Fig. 13. With the increase of heating power of PI films, the time of preheating the battery to 25 °C reduces, while the power consumption increases. When the PI films work

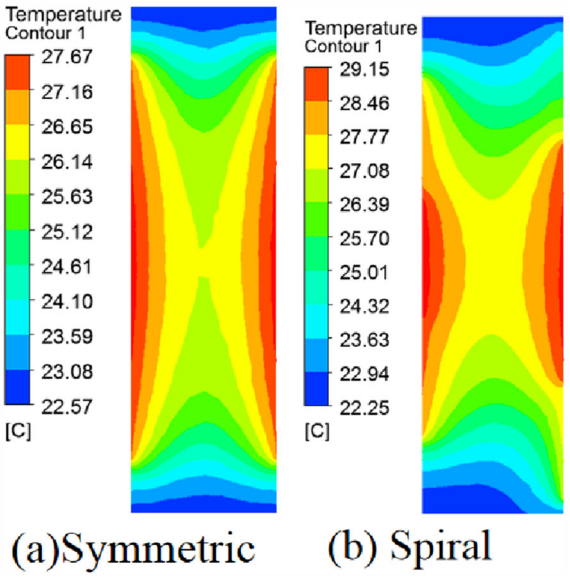

Figure 12. Temperature contours of battery with different layout of heating film.

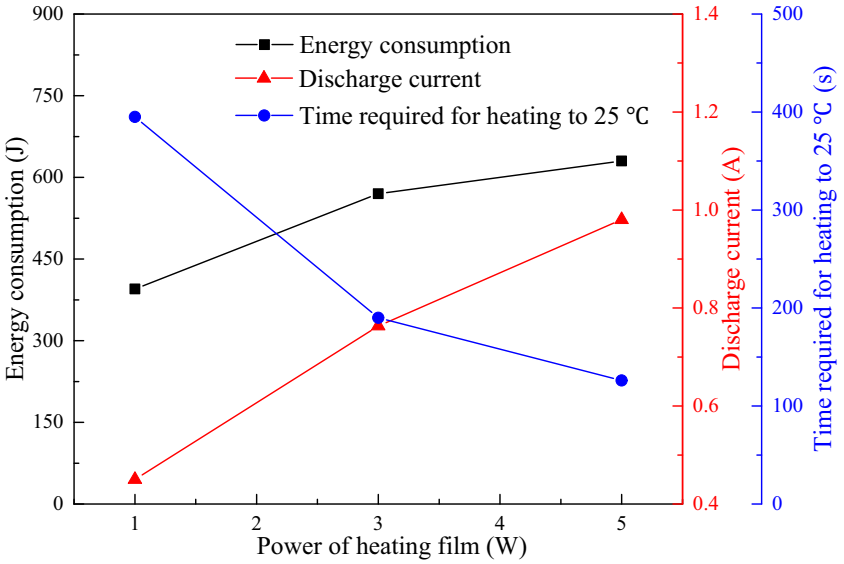

Figure 13. Preheating performance of different power at − 10 °C.

Table 4
Comparison of Parameters Under Different Heating Powers

Power/W	Current/A	Time/s	Consumption/J	ΔT in middle section/°C	ΔT in battery/°C
1	0.44	395	395	1.2	2.6
3	0.76	190	570	2.4	5.2
5	0.99	126	630	3.8	8.5

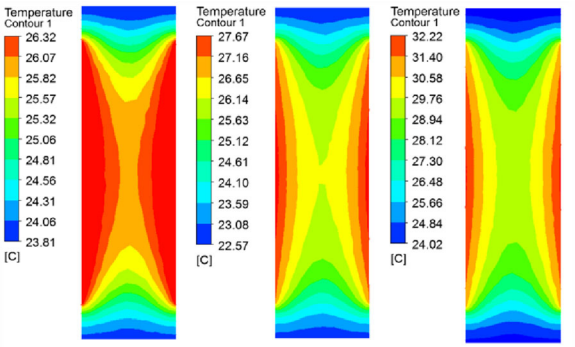

Figure 14. Temperature contours of battery with different heating power.

at 1 W, it takes 395 s to preheat the battery temperature to 25 °C, while 190 s and 126 s are required at 3 W and 5 W, respectively. The temperature difference change is opposite to the change trend of preheating time. As listed in Table 4, with the increase of heating power, the temperature difference of battery increases gradually. In particular, when the heating power is 5 W, the temperature difference on the battery is 8.5 °C. It can be seen that the temperature difference of the battery is caused by the temperature difference between the two sides and the middle of the battery in Fig. 14. Considering preheating time, power consumption and temperature difference, the battery can get good preheating performance when PI films work at 3 W.

5.3. Effect of Preheat Process on Temperature Difference

The battery is discharging during battery preheating, and the increasing of temperature difference will reduce the performance and life of battery. The requirement of battery preheating is that the temperature of the battery is quickly heated to a specific temperature, and the temperature difference is required to be less than 5 °C. It can be seen from the Sect. 5.2 that increasing the power of heating film can reduce the preheating time, while the temperature difference of battery is raised. Thus, different heating powers can be arranged in the heating process, and

Table 5
Different Preheating Process of PI Heating Film

Strategies	Preheat process	Time (s)
Case 1	Preheating the battery with 3 W power for 180 s	180
Case 2	Preheating the battery with 3 W power for 170S, and then preheating the battery with 1 W for 30 s	200
Case 3	Preheating the battery with 5 W power for 100 s, and then \preheating the battery with 1 W for 40 s	140
Case 4	Preheating the battery with 5 W power for 60 s, preheating the battery with 3 W for 60 s, and then preheating the battery with 1 - W power for 60 s	180

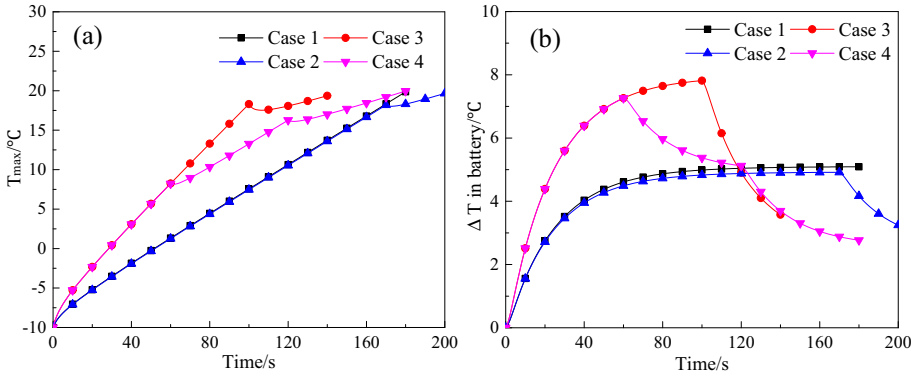

Figure 15. The T_{max} and ΔT in battery change with different preheating process.

the heating speed and temperature difference can be considered comprehensively. The battery is heated at high heating power firstly, and then the heating power is decreased. Four kinds of preheating strategies are described in Table 5 to discuss the effect of preheat process on temperature difference of battery. The power consumptions of four kinds of strategies during preheating are 540 J, which is the power consumption when the heating power is 3 W in heating process. The T_{max} and ΔT in battery change with different preheating process are shown in Fig. 15. The T_{max} of battery is raised quickly and exceeds 20 °C at the end of preheating with different heating strategies. However, the heating time for four kinds of cases is different. The heating time of Case 3 is 140s, shortest among four kinds of strategies, while the preheating times of Case 1, Case 2, and Case 4 are 180 s, 200 s and 180 s, respectively. However, the ΔT value of battery at the end of preheating in Case 4 is lowest, which is 2.8 °C, and the ΔT values of battery for Case 1, Case 2, and Case 3 are 5.1 °C, 3.6 °C and 3.2 °C, respectively. As compared with Case 1, the preheating time and temperature difference of Case 3 are reduced

by 40 s and 1.9 °C. The heating power of the battery is 5 W first in Case 3, and reduces to 1 W subsequently, which can improve the preheating performance comprehensively.

6. Conclusion

To reduce the fire risk of LIBs, battery preheating is important for EVs operation in low temperature environment. In this study, the electro-thermal model and the preheating model of LIBs at low temperature are established and verified based on the second-order ECM, and the temperature changes of battery discharge at low temperatures and preheating with PI heating film are investigated.

(1) The thermal performance of simulation is verified by experiment, and the ECM of battery can adjust the internal parameters according to the SOC and temperature.
(2) When the battery is preheated from − 15 °C to 25 °C, the ohmic resistance of battery decreases from 0.12 Ω to 0.05 Ω at SOC of 0.5.
(3) When the power of symmetrical heating films increases from 1 to 5 W, the heating time reduces from 395 to 126 s, while the power consumption and temperature difference are worsened.
(4) As compared with Case 1, the preheating time and temperature difference of Case 3 are reduce by 40 s and 1.9 °C, which can improve the preheating performance comprehensively.

SUPPLEMENTARY INFORMATION

The online version contains supplementary material available at https://doi.org/10.1007/s10694-022-01251-0.

References

1. Wang C, Chen G, Kou J, Zhang X, Xu X, Bao J, Shen Z, Jin X, Zhang H, Liu L, Yu K (2020) Sb@S–N–C nanocomposite as long-cycle stable anode material for lithium ion batteries. J Alloy Compo 814:152161. https://doi.org/10.1016/j.jallcom.2019.152161
2. Zhou H, Zhou F, Xu L, Kong J, Yang Q (2019) Thermal performance of cylindrical Lithium-ion battery thermal management system based on air distribution pipe. Int J Mass Tran 131:984–998. https://doi.org/10.1016/j.ijheatmasstransfer.2018.11.116
3. Collins GA, Geaney H, Ryan KM (2021) Alternative anodes for low temperature lithium-ion batteries. J Mater Chem A 9:14172–14213. https://doi.org/10.1039/d1ta00998b
4. Xie W, Liu X, He R, Li Y, Gao X, Li X, Peng Z, Feng S, Feng X, Yang S (2020) Challenges and opportunities toward fast-charging of lithium-ion batteries. J Energy Storage 32:101837. https://doi.org/10.1016/j.est.2020.101837
5. Yang X, Duan Y, Feng X, Chen T, Xu C, Rui X, Ouyang M, Lu L, Han X, Ren D, Zhang Z, Li C, Gao S (2020) An experimental study on preventing thermal Runaway

propagation in lithium-ion battery module using aerogel and liquid cooling plate together. Fire Technol 56:2579–2602. https://doi.org/10.1007/s10694-020-00995-x
6. Chen H, Buston JEH, Gill JG, Howard D, Shelke AS (2020) An experimental study on thermal runaway characteristics of lithium-ion batteries with high specific energy and prediction of heat release rate. J Power Sources 472:228585. https://doi.org/10.1016/j.jpowsour.2020.228585
7. Monika K, Chakraborty C, Roy S, Sujith R, Datta SP (2021) A numerical analysis on multi-stage Tesla valve based cold plate for cooling of pouch type Li-ion batteries. Int J Mass Tran 177:121560. https://doi.org/10.1016/j.ijheatmasstransfer.2021.121560
8. Yang W, Zhou F, Liu Y, Xu S, Chen X (2021) Thermal performance of honeycomb-like battery thermal management system with bionic liquid mini-channel and phase change materials for cylindrical lithium-ion battery. Appl Therm Eng 188:116649. https://doi.org/10.1016/j.applthermaleng.2021.116649
9. Dong X, Wang YG, Xia Y (2021) Promoting rechargeable batteries operated at low temperature. Acc Chem Res 54:3883–3894. https://doi.org/10.1021/acs.accounts.1c00420
10. Liu HQ, Wei ZB, He WD, Zhao JY (2017) Thermal issues about Li-ion batteries and recent progress in battery thermal management systems: A review, Energ. Convers. Manage 150:304–330. https://doi.org/10.1016/j.enconman.2017.08.016
11. Liu Y, Xia Y, Zhou Q (2021) Effect of low-temperature aging on the safety performance of lithium-ion pouch cells under mechanical abuse condition: a comprehensive experimental investigation. Energy Storage Mater 40:268–281. https://doi.org/10.1016/j.ensm.2021.05.022
12. Piao N, Gao X, Yang H, Guo Z, Hu G, Cheng H-M, Li F (2022) Challenges and development of lithium-ion batteries for low temperature environments. eTransportation 11:1145. https://doi.org/10.1016/j.etran.2021.100145
13. Chen M, Li J (2021) Experimental study on heating performance of pure electric vehicle power battery under low temperature environment. Int J Mass Tran 172:121191. https://doi.org/10.1016/j.ijheatmasstransfer.2021.121191
14. Li J, Sun D, Chai Z, Jiang H, Sun C (2019) Sinusoidal alternating current heating strategy and optimization of lithium-ion batteries with a thermo-electric coupled model. Energy 186:115798. https://doi.org/10.1016/j.energy.2019.07.128
15. Zhang GS, Ge SH, Xu T, Yang XG, Tian H, Wang CY (2016) Rapid self-heating and internal temperature sensing of lithium-ion batteries at low temperatures. Electrochim Acta 218:149–155. https://doi.org/10.1016/j.electacta.2016.09.117
16. Darcovich K, MacNeil DD, Recoskie S, Kenney B (2018) Coupled electrochemical and thermal battery models for thermal management of prismatic automotive cells. Appl Therm Eng 133:566–575. https://doi.org/10.1016/j.applthermaleng.2018.01.094
17. Wang TZ, Wu XG, Xu SB, Hofmann H, Du JY, Li JQ, Ouyang MG, Song ZY (2018) Performance of plug-in hybrid electric vehicle under low temperature condition and economy analysis of battery pre-heating. J Power Sources 401:245–254. https://doi.org/10.1016/j.jpowsour.2018.08.093
18. Zhu T, Min HT, Yu YB, Zhao ZM, Xu T, Chen Y, Li XY, Zhang C (2017) An optimized energy management strategy for preheating vehicle-mounted Li-ion batteries at Subzero temperatures. Energies 10:243. https://doi.org/10.3390/en10020243
19. Soltani M, Berckmans G, Jaguemont J, Ronsmans J, Kakihara S, Hegazy O, Van Mierlo J, Omar N (2019) Three dimensional thermal model development and validation for lithium-ion capacitor module including air-cooling system. Appl Therm Eng 153:264–274. https://doi.org/10.1016/j.applthermaleng.2019.03.023

20. Zhang J, Sun F, Wang Z (2017) Heating character of a $LiMn_2O_4$ battery pack at low temperature based on PTC and metallic resistance material. Energy Procedia 105:2131–2138. https://doi.org/10.1016/j.egypro.2017.03.602
21. Lei Z, Zhang C, Li J, Fan G, Lin Z (2015) Preheating method of lithium-ion batteries in an electric vehicle. J Mod Power Syst Clean Energy 3:289–296. https://doi.org/10.1007/s40565-015-0115-1
22. Zhang J, Liu H, Zheng M, Chen M, Zhao L, Du D (2021) Numerical study on a preheating method for lithium-ion batteries under cold weather conditions using phase change materials coupled with heat films. J Energy Storage. https://doi.org/10.1016/j.est.2021.103651
23. Kirad K, Chaudhari M (2021) Design of cell spacing in lithium-ion battery module for improvement in cooling performance of the battery thermal management system. J Power Sources 481:229016. https://doi.org/10.1016/j.jpowsour.2020.229016
24. Zhu J, Knapp M, Darma MSD, Fang Q, Wang X, Dai H, Wei X, Ehrenberg H (2019) An improved electro-thermal battery model complemented by current dependent parameters for vehicular low temperature application. Appl Energy 248:149–161. https://doi.org/10.1016/j.apenergy.2019.04.066
25. Yang H, Sun X, An Y, Zhang X, Wei T, Ma Y (2019) Online parameters identification and state of charge estimation for lithium-ion capacitor based on improved Cubature Kalman filter. J Energy Storage 24:100810. https://doi.org/10.1016/j.est.2019.100810
26. Zhou H, Zhou F, Zhang Q, Wang Q, Song Z (2019) Thermal management of cylindrical lithium-ion battery based on a liquid cooling method with half-helical duct. Appl Therm Eng 162:114257. https://doi.org/10.1016/j.applthermaleng.2019.114257
27. Zhang H, Li C, Zhang R, Lin Y, Fang H (2020) Thermal analysis of a 6s4p Lithium-ion battery pack cooled by cold plates based on a multi-domain modeling framework. Appl Therm Eng 173:115216. https://doi.org/10.1016/j.applthermaleng.2020.115216
28. Zhao J, Rao Z, Li Y (2015) Thermal performance of mini-channel liquid cooled cylinder based battery thermal management for cylindrical lithium-ion power battery. Energy Convers Manag 103:157–165. https://doi.org/10.1016/j.enconman.2015.06.056
29. Yang W, Zhou F, Zhou H, Liu Y (2020) Thermal performance of axial air cooling system with bionic surface structure for cylindrical lithium-ion battery module. Int J Mass Tran 161:120307. https://doi.org/10.1016/j.ijheatmasstransfer.2020.120307